Volume 16 | Number 17 | 7 May 2014 | Pages 3441–3634

CrystEngComm

www.rsc.org/crystengcomm

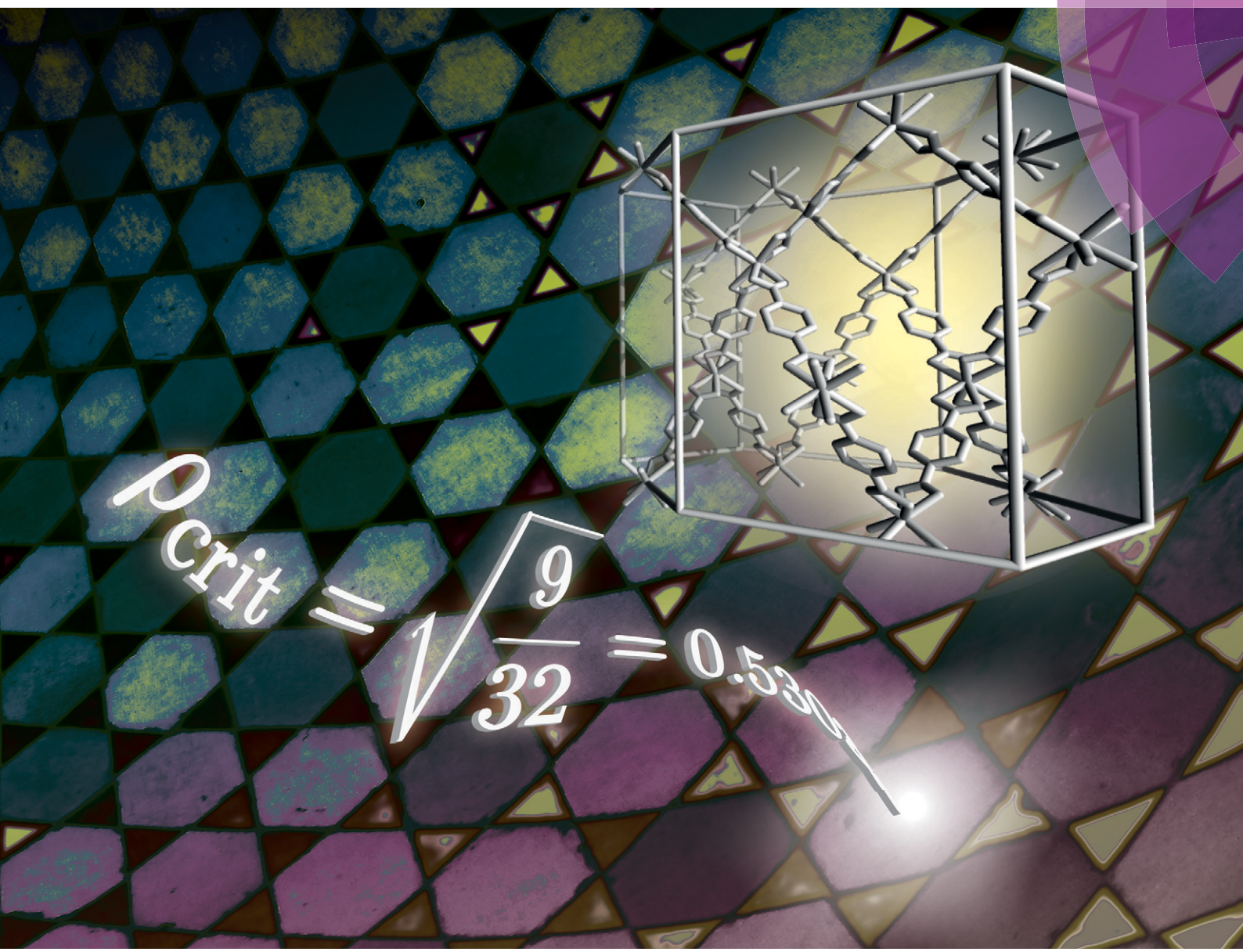

ROYAL SOCIETY OF CHEMISTRY

COVER ARTICLE

Goodwin *et al.*

Geometric switching of linear to area negative thermal expansion in uniaxial metal–organic frameworks

CrystEngComm

PAPER

View Article Online
View Journal | View Issue

Cite this: *CrystEngComm*, 2014, **16**, 3498

Geometric switching of linear to area negative thermal expansion in uniaxial metal–organic frameworks†

Ines E. Collings,[a] Matthew G. Tucker,[b] David A. Keen[b] and Andrew L. Goodwin*[a]

Received 25th October 2013,
Accepted 20th January 2014

DOI: 10.1039/c3ce42165a

www.rsc.org/crystengcomm

Using variable-temperature neutron powder diffraction measurements, we show that the two quartz-like metal–organic frameworks (MOFs) deuterium indium(III) terephthalate and zinc(II) isonicotinate exhibit anisotropic positive and negative thermal expansion (PTE/NTE) behaviour. Whereas in the former the NTE response is uniaxial—occurring along the hexagonal crystal axis—this behaviour is inverted in the latter such that PTE occurs along the hexagonal axis and NTE is found in the entire plane of perpendicular directions. We show that this inversion of mechanical response can be explained on geometric grounds alone; specifically, we identify a critical framework geometry that demarcates a switch from linear to area NTE response. Extending this analysis to other common MOF topologies, we establish a generic predictive approach for establishing the dimensionality of NTE (or, by extension, negative compressibility) responses in a large range of different framework systems. Our analysis suggests that framework geometry plays a crucial role in determining the mechanical response of framework materials which show anisotropic responses *via* hinging.

1. Introduction

Anomalous mechanical responses such as negative thermal expansion (NTE),[1,2] negative linear compressibility (NLC)[3–5] and auxetic behaviour[6–10] are highly desirable targets in the design of new materials with advanced properties.[11] For example, NTE—whereby a material contracts upon heating—can be used to produce thermal-expansion-adjustable composites for application in diffraction gratings and optical fibres.[11] Likewise, NLC and auxetic responses are attractive mechanics in the development of high-performance pressure sensors,[12] and artificial muscles.[13,14] NLC involves expansion in one direction upon uniform compression and is related to auxetic behaviour. The latter entails lateral contraction under axial compression, as occurs in materials with a negative Poisson's ratio (NPR) [Fig. 1].

In the field of engineering, specific beam structures—such as the "honeycomb", "re-entrant honeycomb" and "wine-rack" networks—are known to exhibit these negative responses.[12,15–19] For each of these systems, it is now well-established that it is not only the connectivity of the network but the angles between connecting beams (*i.e.* network geometry) that are crucial in determining mechanical response.[20–23] For example, the specific geometry of a honeycomb net determines whether the system has a positive or negative Poisson's ratio [Fig. 1(d)].

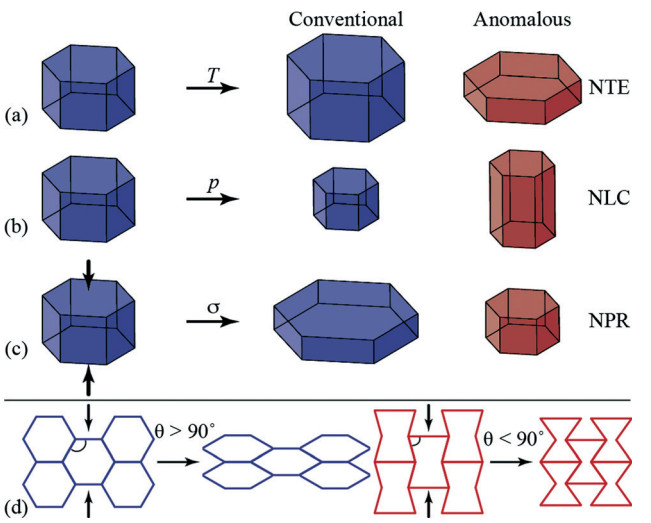

Fig. 1 Diagrammatic representation of anomalous mechanics for materials exhibiting (a) uniaxial negative thermal expansion (NTE); contraction in one direction upon heating, (b) negative linear compressibility (NLC); expansion in one direction under hydrostatic pressure, and (c) auxetic response upon axial compression (indicated by the arrows), whereby a negative Poisson's ratio (NPR) is observed. (d) Honeycomb frameworks with different geometries (framework angles) exhibit contrasting mechanical responses to axial compression.

[a] *Inorganic Chemistry Laboratory, Department of Chemistry, University of Oxford, South Parks Road, Oxford, OX1 3QR, UK. E-mail: andrew.goodwin@chem.ox.ac.uk*
[b] *ISIS Facility, Rutherford Appleton Laboratory, Harwell Oxford, Didcot, Oxfordshire, OX11 0QX, UK*

† Electronic supplementary information (ESI) available: Rietveld refinements, atomic coordinates, lattice parameter data and framework angle derivation. See DOI: 10.1039/c3ce42165a

From a materials chemist's perspective, it is tempting then to begin exploiting the role of network geometry within framework design, so that new structures with desirable intrinsic functionalities can be targeted. To date, much of the design focus has been concerned with systematic variation in network composition or network topology. For example, tailoring of mechanical behaviour has been achieved by (i) transition metal substitution in formate-based metal–organic frameworks (MOFs)[24] and Prussian blue analogues,[25,26] and (ii) exploiting different topologies in zeolitic imidazolate frameworks[27] and transition metal terephthalates (MIL family).[28,29] Yet the enormous structural diversity found in MOFs offers an attractive opportunity to explore not just the roles of chemistry and topology, but also the way in which framework geometry affects mechanical response. Such a strategy might help establish whether in framework materials—as in engineering beam structures—even the angles between network linkers can play a dominant role in determining anomalous negative responses such as NTE and NLC.

Our approach is to study two MOFs with the same topology but with contrasting geometries: zinc(II) isonicotinate, $Zn(ISN)_2$ (ISN = isonicotinate, or pyridine-4-carboxylate),[30,31] and deuterium indium(III) terephthalate, $InD(BDC)_2$ (BDC = 1,4-benzenedicarboxylate or terephthalate)[30] [Fig. 2]. In both cases, their hexagonal framework structures are described by a set of tetrahedral nodes (Zn^{2+} or In^{3+}), linked *via* molecular anions (ISN^- or BDC^{2-}) to form doubly-interpenetrated quartz nets. The differing geometry is evident in a marked contrast in c/a ratios that arises from the intraframework angles. Using variable-temperature diffraction measurements, we determined the thermo-mechanical response of these two MOFs. We find that geometric differences are actually sufficient to invert the response in the two frameworks. On heating, $Zn(ISN)_2$ contracts in the (a,b)-plane and expands along the c-axis, whereas $InD(BDC)_2$ expands in the (a,b)-plane but contracts along the c-axis. Not only do we identify these potentially useful NTE responses, but we show that the inversion in anisotropy between the two materials can actually be rationalised purely in terms of a simple geometric formalism. Our study concludes with a discussion of how our analysis might be generalised to other framework topologies, and predicts a similar switch from uniaxial to area-NTE (or NLC) in a number of topical MOF families.

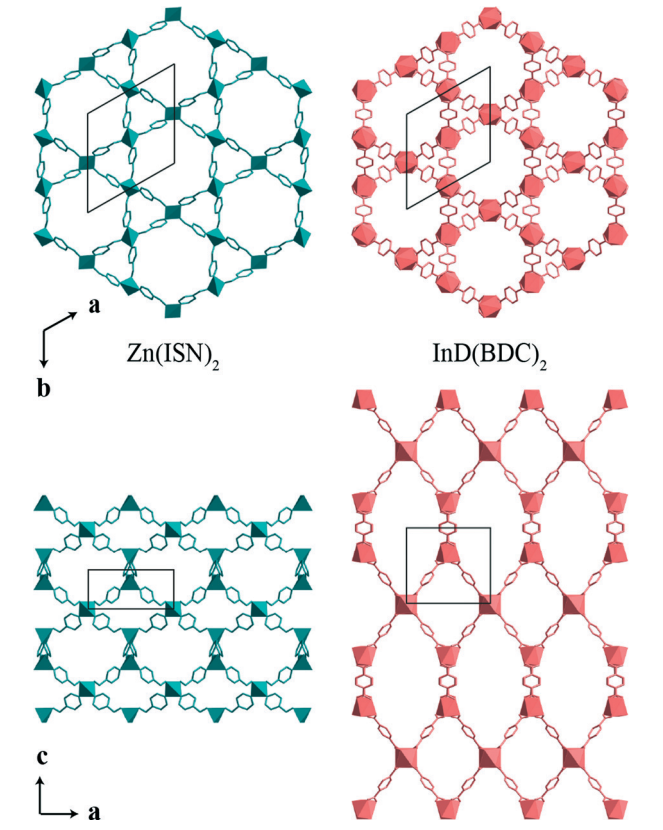

Fig. 2 Representations of the extended framework structures of $Zn(ISN)_2$ and $InD(BDC)_2$ with metal coordination environments shown as polyhedra. The second interpenetrating net has been removed for clarity. Two views are shown: firstly to show their topological similarity to quartz (top), and secondly to highlight their different geometries (c/a ratio; bottom).

2. Methods

Variable-temperature neutron powder diffraction experiments were carried out as part of a broader study into the interplay between the dynamics and flexibility of MOFs,[32] and hence deuterated MOFs were synthesised. A polycrystalline sample of zinc(II) isonicotinate was prepared by mixing stoichiometric quantities of $Zn(CH_3COO)_2{\cdot}2H_2O$ (Sigma Aldrich, 98%) and isonicotinic-d^4 acid (QMx, 98% D) dissolved in dimethylsulfoxide (Sigma Aldrich, 99.5%). The white polycrystalline precipitate which was formed was filtered, washed and dried *in vacuo* (100 °C, 24 h) in order to remove solvent from the framework pores.[30]

Deuterium indium(III) terephthalate was prepared *via* hydrothermal synthesis. $InCl_3$ (Sigma Aldrich, 99.999%) and terephthalic-d^4 acid (Sigma Aldrich, 98% D) were dissolved in dimethylformamide (Sigma Aldrich, 99.9%) and left stirring for 24 h. A small quantity of insoluble impurities was removed by filtration. D_2O (Sigma Aldrich, 99.9% D) was added to the solution over gentle heating (60 °C) to allow H^+/D^+ exchange of mobile protons. The solution was then placed in a 300 ml Teflon-lined bomb and heated in an oven at 160 °C for 3 days. The white polycrystalline gel so formed was isolated by filtration, washed and dried *in vacuo* (100 °C, 24 h) in order to remove solvent from the framework pores.[30] Working within a glovebox, the dried samples (*ca.* 2 g) were ground and transferred to vanadium cans suitable for neutron scattering measurements. In practice we found evidence that some solvent remained within each framework (see ESI†); throughout our manuscript the notation $Zn(ISN)_2$ and $InD(BDC)_2$ should be taken to mean $Zn(ISN)_2{\cdot}\{guest\}$ and $InD(BDC)_2{\cdot}\{guest\}$.

Neutron powder diffraction data were collected on warming at temperatures of 10 K, 50 K and then at intervals of 50 K up to 300 K for $Zn(ISN)_2$ and $InD(BDC)_2$ using the time-of-flight

diffractometer GEM at ISIS.[33–35] For the experiment, 1.9 g of $Zn(ISN)_2$ and 1.5 g of $InD(BDC)_2$, prepared as described above, were each placed within cylindrical vanadium cans of 8.3 mm diameter and 6 cm height. Both cans were loaded at room temperature inside a closed cycle helium refrigerator and the temperature was lowered to 10 K for the start of the measurement.

The experimental diffraction profiles were fitted using the TOPAS refinement program (Topas Academic Version 4.1)[36] using the published models as a starting point.[30,31] For $Zn(ISN)_2$, atomic coordinates of the isonicotinate ligand were refined using rigid body constraints in order to minimise the number of refineable parameters; likewise a single set of anisotropic thermal parameters was refined for all atoms in the isonicotinate group. The zinc atom coordinates were kept fixed due to its special position in the (x,y)-plane, and the lack of unique origin along the z-axis, while an isotropic displacement parameter was freely refined. For $InD(BDC)_2$, atomic coordinates of the terephthalate moiety were refined using a combination of rigid body constraints and distance restraints, and a single set of isotropic thermal parameters was refined for all atoms in the terephthalate group. The indium atom coordinates were kept fixed due to it being on a special position in all crystallographic directions, while an isotropic displacement parameter was freely refined. Rietveld fits are provided as ESI,† as well as additional discussion regarding the incomplete desolvation of the frameworks, which we show does not affect the results of our analysis.

3. Results

Our variable-temperature neutron powder diffraction patterns of perdeuterated samples of $Zn(ISN)_2$ and $InD(BDC)_2$ could be fitted using the structural models reported in ref. 30 and 31. In these papers, two different crystal symmetries have been proposed for $Zn(ISN)_2$: namely, $P3_1$ and $P6_2$. We have used the $P6_2$ model of ref. 31 as our refinements did not show any evidence of symmetry lowering; representative Rietveld fits are given as ESI [Fig. S1].†

Relative changes in the lattice parameters extracted from these fits are shown in Fig. 3. These data are fitted using an empirical equation of the form

$$\ell(T) = \ell_0 + \kappa T[T/(T + T_c)]^{\lambda}, \quad (1)$$

which helps capture the nonlinearity at low temperatures.[37] The slope of these fits corresponds to the expansivities along the different crystal axes, and is quantified by the coefficient of thermal expansion $\alpha_\ell = \mathrm{d}(\ln \ell)/\mathrm{d}T$. The values of α_a and α_c extracted using linear fits to these data are given in Table 1, while the expansivities calculated using the derivative of eqn (1) are shown in Fig. 3. The magnitudes of these coefficients of thermal expansion are often large with respect to oxide-based frameworks (*cf.* $\alpha = -9.1$ MK^{-1} in ZrW_2O_8; ref. 38), but are consistent with the extreme values increasingly observed for MOFs.[37,39–41] The volume expansivities are not especially large because the positive thermal expansion (PTE) in one direction is always balanced by NTE in another direction. The fundamental difference between the two systems is that this NTE is observed along different axes: $Zn(ISN)_2$ exhibits biaxial NTE in the (a,b)-plane (area expansivity $\alpha_A = 2\alpha_a = -21.8(10)$ MK^{-1}), and $InD(BDC)_2$ displays uniaxial NTE along the c-axis ($\alpha_c = -35(2)$ MK^{-1}). Actually, biaxial NTE is a rare phenomenon having been reported in just a handful of materials: the few examples include (*S*,*S*)-octa-3,5-diyn-2,7-diol,[42]

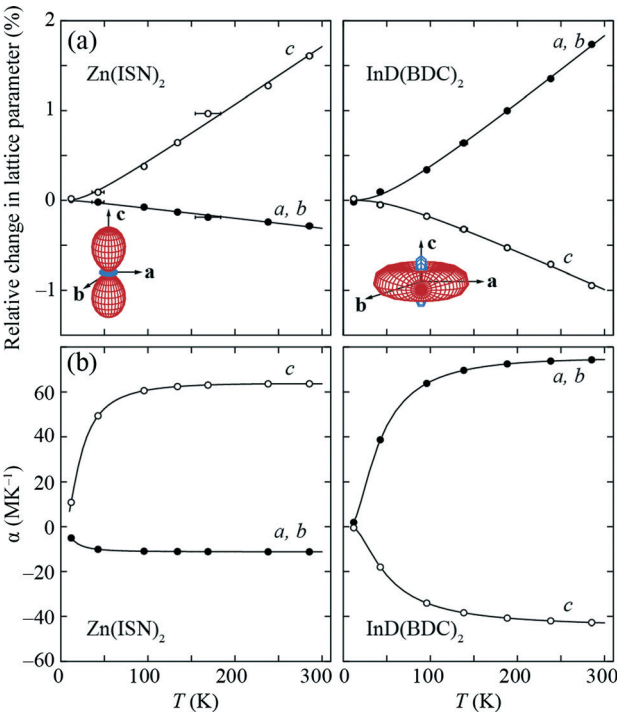

Fig. 3 (a) Thermal variation in lattice parameters and (b) the corresponding thermal expansivities observed for $Zn(ISN)_2$ and $InD(BDC)_2$ over the temperature range 10–300 K. We note that the large error in the 170 K $Zn(ISN)_2$ temperature point arises from a difficulty in thermal stabilisation at this temperature for the closed cycle helium refrigerator used in the experiment. Errors are substantially minimised in $InD(BDC)_2$ as equilibration time was extended. The expansivity indicatrix for each MOF is shown as an inset to (a) and indicates the spatial orientation of positive (red) and negative (blue) thermal expansion axes.[43]

Table 1 Thermal expansivities of the unit cell and geometric parameters of $Zn(ISN)_2$ and $InD(BDC)_2$, calculated using linear fits to data

	α_i (MK^{-1})	
Parameter, i	$Zn(ISN)_2$	$InD(BDC)_2$
a,b	−10.9(5)	64(3)
c	60(3)	−35(2)
V	37.8(18)	94(4)
r	4.7(4)	9.2(3)
θ_1	26.3(11)	−41(2)
θ_2	6.9(3)	−15.9(8)
θ_3	−27.0(12)	68(3)

the MOF Cu-SIP-3,[43] $Ni(CN)_2$,[44] Zn(4-(1*H*-naphtho[2,3-*d*]imidazol-1-yl)benzoate)$_2$,[41] and silver tricyanomethanide.[45]

Throughout the large and contrasting responses of $Zn(ISN)_2$ and $InD(BDC)_2$ to changes in temperature, we find that the distance r between connected metal centres remains essentially constant [Fig. 4(a)]; *i.e.* covalent bond lengths are conserved. Instead the structural changes are dominated by large variations in framework angles. There are three unique framework angles in the β-quartz topology [θ_1, θ_2, θ_3 in Fig. 4(a)] that are related to each other in a complex manner (see ESI†). The change in these framework angles with temperature can be quantified in a similar way to lattice expansivities by denoting

$$\alpha_\theta = \frac{1}{\theta}\frac{\mathrm{d}\theta}{\mathrm{d}T}. \tag{2}$$

The magnitudes of the α_{θ_i} can be very much larger than α_r (Table 1), supporting the interpretation that geometric flexing of the framework dominates the bulk lattice parameter evolution [Fig. 4(b)]. A similar hinging mechanism has been observed in many other MOFs.[37,39,41,46,47] The switch in sign of the lattice expansivities between the two frameworks is seen also in the signs of the α_{θ_i}. Yet in both cases the PTE outweighs the NTE observed, and therefore there is an overall positive volume thermal expansion; *i.e.* $\alpha_V > 0$.

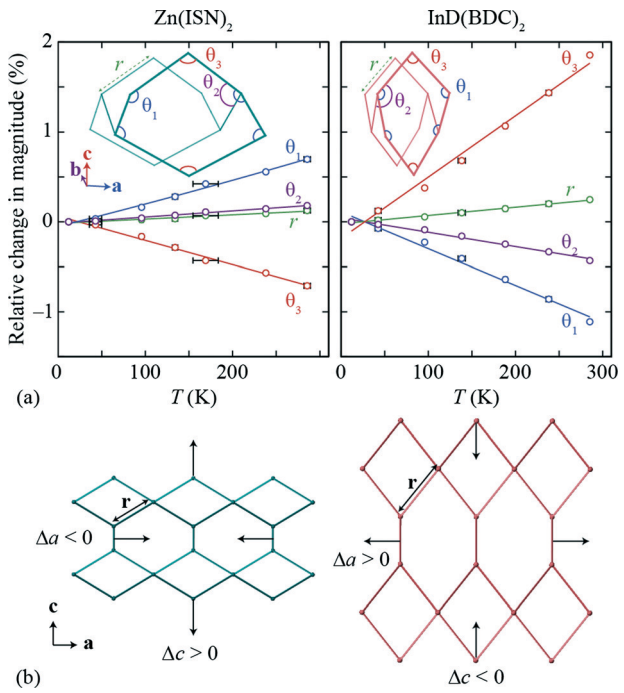

Fig. 4 (a) Thermal variation in the M–ligand–M linker distance r and corresponding framework angles θ_i as a function of temperature. The inset figure shows the location of the angles within the framework structure. (b) Schematic representation of the $Zn(ISN)_2$ and $InD(BDC)_2$ nets. Here ligands are omitted and instead rods indicate the connectivity of the framework. The arrows indicate the direction of expansion or contraction and the linking **r** vector is indicated on both structures.

We proceed now to show that the switch from uniaxial to biaxial NTE can be explained purely on geometric grounds. We use as our basis the pair of observations that $\alpha_r \simeq 0$ and α_V is positive. Our starting point is to define the linking vector **r**—which represents the M–ligand–M unit of the framework—in terms of the lattice vectors **a**, **b**, **c**: in the case of $Zn(ISN)_2$ and $InD(BDC)_2$ we have

$$\mathbf{r} = \frac{1}{2}\mathbf{a} + \frac{1}{2}\mathbf{b} + \frac{2}{3}\mathbf{c}. \tag{3}$$

The magnitude of this vector

$$r = \sqrt{\frac{a^2}{4} + \frac{4c^2}{9}} \tag{4}$$

corresponds to the unique metal–metal distance plotted in Fig. 4(a).‡ Taking the variation in r with T to be small (*i.e.* $\alpha_r = 0$) we have the constraint

$$\alpha_r = 0 = \frac{1}{r}\frac{\mathrm{d}r}{\mathrm{d}T} = \frac{1}{r^2}\left[\frac{a^2\alpha_a}{4} + \frac{4c^2\alpha_c}{9}\right], \tag{5}$$

and hence

$$\alpha_c = -\frac{9}{16\rho^2}\alpha_a, \tag{6}$$

where $\rho = \frac{c}{a}$. It follows that α_a and α_c must have opposite signs, and that the magnitude of one fixes the magnitude of the other for any given value of ρ. In hexagonal systems, $\alpha_V = 2\alpha_a + \alpha_c$, and so the constraint $\alpha_V > 0$, taken with the relationship established in eqn (6), gives the crucial inequality

$$\alpha_V = \alpha_a\left[2 - \frac{9}{16\rho^2}\right] > 0. \tag{7}$$

The importance of this equation is that α_a is predicted to be negative for values $\rho < \sqrt{\frac{9}{32}} = 0.53 = \rho_{\mathrm{crit}}$ and positive whenever ρ is larger than this value. In other words, the geometry of the network determines whether NTE is shown within the (a,b)-plane ($\rho < \rho_{\mathrm{crit}}$) or along the c-axis ($\rho > \rho_{\mathrm{crit}}$).

The experimental values of ρ for $Zn(ISN)_2$ and $InD(BDC)_2$ are given in Table 2, from which it is clear that these two frameworks lie on either side of the value of ρ_{crit} determined above. Consequently, the reversal of anisotropic response to

‡ We note that while there is no unique choice amongst the symmetry-equivalent vectors **r** taken to describe the M–ligand–M linkages in these frameworks, the magnitude of any such vector is identical and is given by eqn (4).

Table 2 Lattice parameters and observed c/a ratios for $Zn(ISN)_2$ and $InD(BDC)_2$ at 285 K

MOF	a (Å)	c (Å)	$\rho = c/a$
$Zn(ISN)_2$	15.4752(6)	6.2254(6)	0.40
$InD(BDC)_2$	14.7860(17)	12.155(3)	0.82

temperature has no real chemical origin, but is a function of geometry alone. Making use of the experimental values of α_V known for $Zn(ISN)_2$ and $InD(BDC)_2$, eqn (7) allows calculation of the coefficients of thermal expansion (CTE) for differing lattice geometries ρ [Fig. 5]. The observed experimental values of CTE for $Zn(ISN)_2$ and $InD(BDC)_2$ are shown as points at the corresponding ρ values; the difference between these points and the calculated lines of CTE reflects the subtle change in the magnitude of r as a function of temperature (which is not accounted for in the above analysis). Hence, if α_r is sufficiently large, it may negate any geometry-driven response. For completeness, we note that the divergence in calculated α values evident near $\rho = \rho_{crit}$ reflects the fact that geometric flexing of a framework with $\rho = \rho_{crit}$ actually results in zero volume change (to first order). Consequently the magnitude of uniaxial expansivities required to give a nonzero volume coefficient of thermal expansion diverges at this point. In practice what this means is that the mechanical response of materials with $\rho = \rho_{crit}$ will not be dominated by geometric flexing, but rather by the intrinsic response of the constituent framework linkers. Nevertheless the design strategy of choosing materials with values of ρ very close to ρ_{crit} may be a useful approach for identifying candidate compounds with extreme linear coefficients of thermal expansion.

We anticipate that this type of geometric analysis may find application in predicting the mechanics of many flexible framework materials, where the changes in network angles dominate the mechanical response. In the discussion below, we proceed to demonstrate how the analysis might be applied to a variety of different systems.

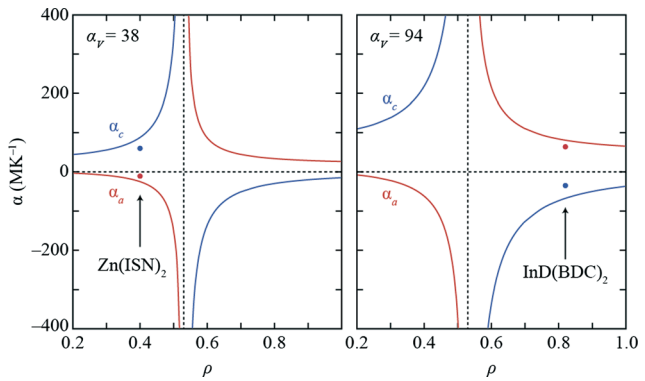

Fig. 5 Calculated coefficients of thermal expansion for the a and c-axes at different values of ρ for $Zn(ISN)_2$ and $InD(BDC)_2$ with constant volume expansion determined from experiment. The points indicate the experimentally-obtained coefficients of thermal expansion. The vertical dashed line marks ρ_{crit}.

4. Discussion

We start by considering other frameworks with the quartz topology, as summarised in Table 3. Following the approach outlined above, a range of critical values of ρ are determined for these different systems. This is perhaps counterintuitive as one might expect a unique critical c/a ratio for a given topology. The origin of this variation lies in the way interpenetration affects the relationship between the linking vector **r** and the lattice vectors. For example, the critical values of ρ in $InD(BDC)_2$ and β-quartz are related by a factor of two because two-fold interpenetration in the former gives rise to a halving of the c lattice parameter [Fig. 6]. For all the frameworks listed in Table 3, with the exception of $Zn(ISN)_2$, the observed value of ρ lies above ρ_{crit}. Consequently we would predict that they should all show NTE along their c-axes, as is indeed found to be the case experimentally. So the differing chemistry of these frameworks would seem not to affect the anisotropy in lattice parameter evolution, but rather only the magnitude of mechanical response. We comment that the inclusion of a silica polymorph in Table 3 is purely for reference; we are not advocating that geometry plays a more significant role in this system than do other deformation modes.[48,49]

The framework material $Zn[Ag(CN)_2]_2{\cdot}AgCN$ shown in Table 3 is a somewhat complex example, because it exhibits modest volume NTE ($\alpha_V < 0$) despite the fact that its uniaxial response is as one would expect for a system with positive volume thermal expansion. This apparent discrepancy arises because the framework thermal expansion is dominated by the NTE behaviour of the linkers (strong because of low-energy transverse vibrations) rather than by geometric flexing of the lattice (weak because of the presence of AgCN chains within the framework pores). The geometric contribution to the volume expansivity

$$\begin{aligned}\alpha_{V,\mathrm{geom}} &= \alpha_V - 3\alpha_r \\ &= -13.57(29)\,\mathrm{MK}^{-1} - 3\times(-5.02(14)\,\mathrm{MK}^{-1}) \\ &= +1.5(5)\,\mathrm{MK}^{-1}\end{aligned} \quad (8)$$

is positive and consequently the direction of uniaxial response, which is governed by geometry, is as expected for a system that exhibits volumetric PTE.[51] We expect that such considerations will be of relevance to only relatively few systems, since the NTE effect associated with transverse vibrational motion is usually much weaker than the NTE/PTE effects associated with framework flexing.[37]

So far our discussion has focused on the interplay between network geometry and *thermal expansivity*, but the analysis we present is equally applicable to understanding anisotropic *compressibility*. Materials with negative compressibilities—a rarer phenomenon than NTE—are attracting substantial interest in the development of sensors and actuators.[12,52] While thermodynamics prohibit a negative volume compressibility (noting, however, the suggestion in ref. 53 that such behaviour might be observable in non-equilibrium foams), the phenomenon

Table 3 Quartz-like frameworks with their unit cells compared to that of β-quartz, the critical and observed ρ values, and coefficients of thermal expansion for the *a* and *c*-axes. The calculated ρ_{crit} values are all related to the β-quartz value of 1.06 by simple exact ratios that reflect the relationship between the corresponding unit cells

Framework	a/a_{SiO_2}	c/c_{SiO_2}	ρ_{crit}	ρ	α_a (MK^{-1})	α_c (MK^{-1})	Ref.
β-quartz	1	1	1.06	1.09	0.12	−1.1	50
$Zn(ISN)_2$	1	0.5	0.53	0.40	−10.9	60	This work
$InD(BDC)_2$	1	0.5	0.53	0.82	64	−35	This work
$Zn[Au(CN)_2]_2$	$1/\sqrt{3}$	1	1.84	2.44	36.9	−57.6	51
$Zn[Ag(CN_2)]_2$[a]	$1/\sqrt{3}$	1	1.84	1.92	4.1	−21.7	51

[a] $Zn[Ag(CN)_2]_2$ contains AgCN within its pores.[51]

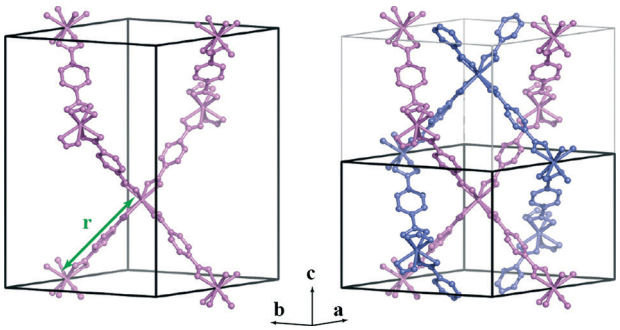

Fig. 6 Relationship between the unit cells of a single net of the quartz-like $InD(BDC)_2$ structure and the observed doubly-interpenetrated net. The unit cell halves along the *c*-axis as a result of interpenetration, which accounts for the factor of two difference in ρ_{crit} values for β-quartz and $InD(BDC)_2$.

of negative area compressibility (NAC) is certainly realisable, as has recently been demonstrated in the coordination polymer silver(I) tricyanomethanide.[45] Just as geometry determines the balance between linear and area NTE, so too might geometric considerations help identify the most likely NAC candidates. Based on the results summarised in Table 3, we would suggest that $Zn(ISN)_2$ is the most likely of these quartz-like frameworks to exhibit NAC. Negative area responses offer two key opportunities: first, coupling of pore widening with volume reduction in principle allows for negative volumes of guest sorption (*i.e.* volume contraction during solvent uptake); and, second, NAC materials increase their surface area under hydrostatic pressure, and so they can be used as substrates to provide order-of-magnitude amplification of piezoelectric response in *e.g.* ferroelectric sensors.[6]

Our approach is not limited to quartz-like frameworks. It might usefully be applied to any uniaxial system (trigonal, hexagonal or tetragonal), where the following two considerations are satisfied: (*i*) geometric changes are likely to dominate lattice parameter evolution, and (*ii*) all linking vectors **r** are related to each other and to the lattice vectors **a**, **b**, **c** by symmetry considerations. While in the case of $Zn(ISN)_2$ and $InD(BDC)_2$ α_V is positive, it is possible that certain frameworks will show negative volume expansion. In such cases, the anisotropy prediction will be inverted because the inequality in eqn (7) will switch to fulfil $\alpha_V < 0$; the existence and value of a critical *c*/*a* ratio, however, is unaffected by the sign of the volume coefficient of thermal expansion. We note that while volume NTE has been observed in many framework materials which exhibit transverse vibrational modes of their linker as their main deformation mode,[54–57] frameworks which display hinging mechanisms generally exhibit positive volume thermal expansion.[2,37,39,41,46,47] So we anticipate that the condition $\alpha_V > 0$ will actually hold for the vast majority of frameworks for which geometric hinging is possible. These considerations may be affected also by the presence or otherwise of solvent within framework pores. In the ESI,† we show that the presence of the solvent within the pores of either $Zn(ISN)_2$ or $InD(BDC)_2$ does not affect the direction of anisotropy, influencing instead only the magnitude of response.[41,58] It remains possible, if unlikely, that the inclusion of solvent within the pores of other framework materials induces a sufficiently large change in geometry that a reverse in anisotropic mechanical response arises. In this way, sorption/desorption might be used to trigger a switch from *e.g.* area to linear NTE or *vice versa*.

We proceed to illustrate the generality of our geometric analysis by considering several MOF families. Anisotropic compressibility within the family of ammonium transition-metal formates, $[NH_4][M(HCOO)_3]$ is first examined. These frameworks have the **acs** topology, the parent of which is tungsten carbide. The zinc- and magnesium-containing members have recently been shown to exhibit NLC and NTE, respectively.[47,59] In all cases, the linking vector **r** corresponds to a M–formate–M unit [Fig. 7] and is related to the lattice vectors by the relationship

$$\mathbf{r} = \frac{1}{3}\mathbf{a} - \frac{1}{3}\mathbf{b} + \frac{1}{2}\mathbf{c}. \quad (9)$$

Consequently the linker length is given by

$$r = \sqrt{\frac{a^2}{3} + \frac{c^2}{4}}. \quad (10)$$

We now consider the linear compressibilities of this system, denoted by $K_\ell = -\mathrm{d}(\ln \ell)/\mathrm{d}p$. If geometric variations dominate its mechanical response, then we might make the approximation $K_r \simeq 0$, giving

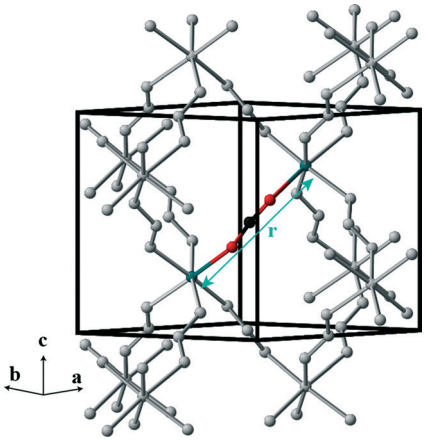

Fig. 7 Representation of the $[NH_4][M(HCOO)_3]$ structure, with the **r** vector highlighted in the coloured M–formate–M link. H atoms have been omitted for clarity.

$$K_r \simeq 0 = -\frac{1}{r}\frac{\mathrm{d}r}{\mathrm{d}p} = -\frac{1}{r^2}\left[\frac{a^2K_a}{3} + \frac{c^2K_c}{4}\right], \quad (11)$$

and hence

$$K_c = -\frac{4}{3\rho^2}K_a. \quad (12)$$

This again predicts that the a and c compressibilities are of opposite signs. Since in general $K_V = 2K_a + K_c > 0$, we obtain the inequality

$$K_a\left[2 - \frac{4}{3\rho^2}\right] > 0, \quad (13)$$

whence K_a is predicted to be negative for values $\rho < \sqrt{\frac{2}{3}} = 0.82 = \rho_{crit}$ and positive for $\rho > \sqrt{\frac{2}{3}}$. The observed ρ value for $[NH_4][Zn(HCOO)_3]$ is 1.12. As this lies above ρ_{crit}, our geometric analysis would predict $K_a > 0$ and $K_c < 0$. The experimental compressibilities given in ref. 47 are K_a = 15.8(9) TPa^{-1} and K_c = −1.8(8) TPa^{-1}. We would expect similar responses for the other ammonium transition-metal formates as the observed ρ does not vary significantly with change in metal and is always above ρ_{crit}: ρ = 1.10 for $[NH_4][Ni(HCOO)_3]$ and ρ = 1.15 for $[NH_4][Mn(HCOO)_3]$.[60] Recently, the $[NH_4][Mg(HCOO)_3]$ framework—for which one obtains the same value of ρ_{crit}—has been shown to exhibit anisotropic thermal expansion. In this case the negative response is again along the c-axis, which is consistent with the observation $\rho = 1.13 > \rho_{crit}$.[59]

Likewise, the MIL-88 family—composed of metallic trimers connected *via* dicarboxylate groups—has the **acs** topology, and hence exhibits the same critical value as above (ρ_{crit} = 0.82; calculated by using the centre of the metal clusters as nodes).[61] Although no variable-pressure or variable-temperature studies have been carried out for these systems, adsorption of small molecules such as water and pyridine into the framework causes volume increase *via* expansion within the (a,b)-plane and contraction along the c-axis.[62] This mechanical response to adsorption is consistent with our geometric analysis: the observed ρ in the MIL-88 family is above ρ_{crit} = 0.82, and hence a negative response is expected for the c-axis. By exploiting the tuneable chemistry of the MIL-88 family, the value of ρ can be varied between 1.31 and 2.31 using different ligands§ and maintaining the same topology.[62] While these all lie above ρ_{crit}, the large variation in ρ suggests ligand substitution to be a more effective strategy for accessing different mechanical responses than is metal exchange.

One particularly clear example of how MOF chemistry might be used to access a variety of geometries for a given topology is provided by the series of known diamondoid MOFs. Table 4 and Fig. 8 illustrate the range of observed ρ values—above and below ρ_{crit}—which can be obtained by varying chemical composition. By identifying structures for which $\rho < \rho_{crit}$, we access frameworks which are predicted to show negative area responses in the (a,b)-plane. Consequently, $In(D_L\text{-cam})_2$, $Cu(2,5\text{-}Me_2pyz)_2$ and $Ag(4\text{-cnpy})_2$ are all likely NAC candidates. Whether or not these materials do in fact exhibit NAC will depend on the extent to which their deformation mechanism under pressure is dominated by changes in geometry rather than compression along the M–linker–M units. Indeed competition between geometric flexing and linker deformation is responsible for a switch between negative and positive linear compressibility in the MOF silver(I) 2-methylimidazolate.[37] With this in mind, one could chemically engineer the linking unit to be more "rigid" by using, for instance, aromatic-based ligands that favour linear M–ligand–M coordination.

Table 4 Diamondoid frameworks with their observed and critical ρ values

Framework	ρ	ρ_{crit}	Ref.
$[Ag(4\text{-cnpy})_2][BF_4]$	0.39[a]	0.50	63
$[Cu(4,4'\text{-bipy})_2][PF_6]$	0.57	0.50	64
$[In(D_L\text{-cam})_2][Pr_4N]$	0.60[a]	1.41	65
$[Cu(2,5\text{-}Me_2pyz)_2][PF_6]$	0.69[a]	1.41	66
$Zn(PT)_2$	1.66	1.41	67
$Co(5\text{-X-2-pymo})_2$	1.69	1.41	68
LiB(mim)	2.17	1.41	69

[a] Denotes frameworks which should exhibit a negative area response in the (a,b)-plane as they fulfill $\rho < \rho_{crit}$. Abbreviations used: 4-cnpy = 4-cyanopyridine, 4,4′-bipy = 4,4′-bipyridyl, D_L-cam = enantiopure camphorate, Pr_4N = tetra-*n*-propylammonium, 2,5-Me_2pyz = 2,5-dimethylpyrazine, PT = 5-propyltetrazole, 5-X-2-pymo = 5-halo-pyrimidin-2-ol (X = Br/I), mim = 2-methylimidazolate.

§ The ρ values are calculated using smallest and largest differences in 'as-synthesised' lattice parameters for MIL-88A and MIL-88C respectively.

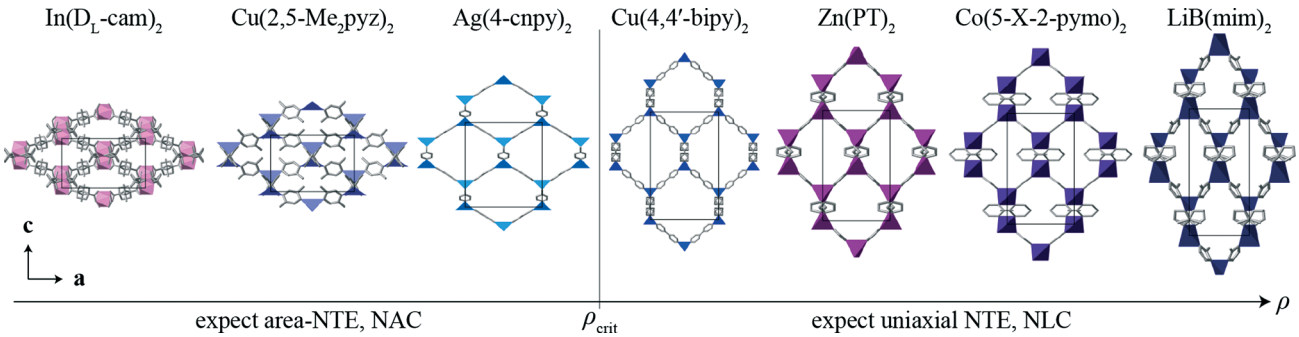

Fig. 8 Extended diamondoid frameworks from Table 4 shown ordered by observed *c*/*a* ratios with the vertical line signifying the critical *c*/*a* value, ρ_{crit}. The observed value of ρ and unit cell dimensions of Ag(4-cnpy)$_2$ and Cu(4,4′-bipy)$_2$ have been scaled by a factor of $2\sqrt{2}$ to allow meaningful comparison with the other frameworks.

5. Conclusions

A straightforward geometric formalism can be used to predict the NTE axis for flexible frameworks of uniaxial crystal symmetry. In particular, we have found that the contrasting geometry in Zn(ISN)$_2$ and InD(BDC)$_2$ gives rise to the switch in anisotropic expansivities. By using geometric considerations, we can formulate a relationship between the sign of the expansivity or compressibility of a crystal axis and the *c*/*a* ratio. Whenever the mechanical response of a MOF is dominated by flexing of its framework structure, we expect that the approach outlined here might be used to predict which frameworks are most likely to show negative area responses to changes in temperature or pressure.

Acknowledgements

This research was supported financially by the EPSRC (grant EP/G004528/2) and the ERC (project 279705), and by the STFC in the form of access to the GEM instrument at ISIS. We are grateful to J. W. Makepeace for assistance with the Topas Academic input files.

References

1 W. Miller, C. W. Smith, D. S. Mackenzie and K. E. Evans, *J. Mater. Sci.*, 2009, **44**, 5441–5451.
2 A. L. Goodwin, M. Calleja, M. J. Conterio, M. T. Dove, J. S. O. Evans, D. A. Keen, L. Peters and M. G. Tucker, *Science*, 2008, **319**, 794–797.
3 R. Gatt and J. N. Grima, *Phys. Status Solidi RRL*, 2008, **2**, 236–238.
4 A. L. Goodwin, D. A. Keen and M. G. Tucker, *Proc. Natl. Acad. Sci. U. S. A.*, 2008, **105**, 18708–18713.
5 A. B. Cairns, J. Catafesta, C. Levelut, J. Rouquette, A. van der Lee, L. Peters, A. L. Thompson, V. Dmitriev, J. Haines and A. L. Goodwin, *Nat. Mater.*, 2013, **12**, 212–216.
6 R. H. Baughman, *Nature*, 2003, **425**, 667.
7 G. N. Greaves, A. L. Greer, R. S. Lakes and T. Rouxel, *Nat. Mater.*, 2011, **10**, 823–837.
8 J. N. Grima, R. Gatt, V. Zammit, J. J. Williams, K. E. Evans, A. Alderson and R. I. Walton, *J. Appl. Phys.*, 2007, **101**, 086102.
9 M. Bouakba, A. Bezazi and F. Scarpa, *Int. J. Solids Struct.*, 2012, **49**, 2450–2459.
10 Z. A. D. Lethbridge, R. I. Walton, A. S. Marmier, C. W. Smith and K. E. Evans, *Acta Mater.*, 2010, **58**, 6444–6451.
11 K. Takenaka, *Sci. Technol. Adv. Mater.*, 2012, **13**, 013001.
12 R. H. Baughman, S. Stafström, C. Cui and S. O. Dantas, *Science*, 1998, **279**, 1522–1524.
13 A. E. Aliev, J. Oh, M. E. Kozlov, A. A. Kuznetsov, S. Fang, A. F. Fonseca, R. Ovalle, M. D. Lima, M. H. Haque, Y. N. Gartstein, M. Zhang, A. A. Zakhidov and R. H. Baughman, *Science*, 2009, **323**, 1575–1578.
14 K. E. Evans and A. Alderson, *Adv. Mater.*, 2000, **12**, 617–628.
15 J. N. Grima, D. Attard, R. Caruana-Gauci and R. Gatt, *Scr. Mater.*, 2011, **65**, 565–568.
16 J. N. Grima, D. Attard and R. Gatt, *Phys. Status Solidi B*, 2008, **245**, 2405–2414.
17 N. Gaspar, X. J. Ren, C. W. Smith, J. N. Grima and K. E. Evans, *Acta Mater.*, 2005, **53**, 2439–2445.
18 J. C. A. Elipe and A. D. Lantada, *Smart Mater. Struct.*, 2012, **21**, 105004.
19 J. Schwerdtfeger, F. Wein, G. Leugering, R. F. Singer, C. Körner, M. Stingl and F. Schury, *Adv. Mater.*, 2011, **23**, 2650–2654.
20 W. Miller, D. S. Mackenzie, C. W. Smith and K. E. Evans, *Mech. Mater.*, 2008, **40**, 351–361.
21 D. L. Barnes, W. Miller, K. E. Evans and A. Marmier, *Mech. Mater.*, 2012, **46**, 123–128.
22 J. N. Grima, R. Caruana-Gauci, D. Attard and R. Gatt, *Proc. R. Soc. London, Ser. A*, 2012, **468**, 3121–3138.
23 T.-C. Lim, *J. Mater. Sci.*, 2012, **47**, 368–373.
24 J.-C. Tan, P. Jain and A. K. Cheetham, *Dalton Trans.*, 2012, **41**, 3949–3952.
25 K. W. Chapman, P. J. Chupas and C. J. Kepert, *J. Am. Chem. Soc.*, 2006, **128**, 7009–7014.
26 S. Adak, L. L. Daemen, M. Hartl, D. Williams, J. Summerhill and H. Nakotte, *J. Solid State Chem.*, 2011, **184**, 2854–2861.
27 J.-C. Tan, T. D. Bennett and A. K. Cheetham, *Proc. Natl. Acad. Sci. U. S. A.*, 2010, **107**, 9938–9943.

28 A. U. Ortiz, A. Boutin, A. H. Fuchs and F.-X. Coudert, *Phys. Rev. Lett.*, 2012, **109**, 195502.
29 A. U. Ortiz, A. Boutin, A. H. Fuchs and F.-X. Coudert, *J. Chem. Phys.*, 2013, **138**, 174703.
30 J. Sun, L. Weng, Y. Zhou, J. Chen, Z. Chen, Z. Liu and D. Zhao, *Angew. Chem., Int. Ed.*, 2002, **41**, 4471–4473.
31 Y. Wu, D. Li, F. Fu, L. Tang, J. Wang and X. G. Yang, *J. Coord. Chem.*, 2009, **62**, 2665–2674.
32 I. E. Collings, M. G. Tucker, D. A. Keen and A. L. Goodwin, *Z. Kristallogr.*, 2012, **227**, 313–320.
33 W. Williams, R. Ibberson, P. Day and J. Enderby, *Phys. B*, 1997, **241–243**, 234–236.
34 P. Day, J. Enderby, W. Williams, L. Chapon, A. Hannon, P. Radaelli and A. Soper, *Neutron News*, 2004, **15**, 19–23.
35 A. C. Hannon, *Nucl. Instrum. Methods Phys. Res., Sect. A*, 2005, **551**, 88–107.
36 A. A. Coelho, *Topas Academic Version 4.1*, Coelho Software, Brisbane.
37 J. M. Ogborn, I. E. Collings, S. A. Moggach, A. L. Thompson and A. L. Goodwin, *Chem. Sci.*, 2012, **3**, 3011–3017.
38 T. A. Mary, J. S. O. Evans, T. Vogt and A. W. Sleight, *Science*, 1996, **272**, 90–92.
39 L. D. DeVries, P. M. Barron, E. P. Hurley, C. Hu and W. Choe, *J. Am. Chem. Soc.*, 2011, **133**, 14848–14851.
40 C. Yang, X. Wang and M. A. Omary, *Angew. Chem., Int. Ed.*, 2009, **48**, 2500–2505.
41 I. Grobler, V. J. Smith, P. M. Bhatt, S. A. Herbert and L. J. Barbour, *J. Am. Chem. Soc.*, 2013, **135**, 6411–6414.
42 D. Das, T. Jacobs and L. J. Barbour, *Nat. Mater.*, 2010, **9**, 36–39.
43 M. J. Cliffe and A. L. Goodwin, *J. Appl. Crystallogr.*, 2012, **45**, 1321–1329.
44 S. J. Hibble, A. M. Chippindale, A. H. Pohl and A. C. Hannon, *Angew. Chem., Int. Ed.*, 2007, **46**, 7116–7118.
45 S. A. Hodgson, J. Adamson, S. J. Hunt, M. J. Cliffe, A. B. Cairns, A. L. Thompson, M. G. Tucker, N. P. Funnell and A. L. Goodwin, *Chem. Commun.*, 2014, DOI: 10.1039/C3CC47032F.
46 Y. Liu, J.-H. Her, A. Dailly, A. J. Ramirez-Cuesta, D. A. Neumann and C. M. Brown, *J. Am. Chem. Soc.*, 2008, **130**, 11813–11818.
47 W. Li, M. R. Probert, M. Kosa, T. D. Bennett, A. Thirumurugan, R. P. Burwood, M. Parinello, J. A. K. Howard and A. K. Cheetham, *J. Am. Chem. Soc.*, 2012, **134**, 11940–11943.
48 L. Huang and J. Kieffer, *Phys. Rev. Lett.*, 2005, **95**, 215901–215904.
49 F. S. Tautz, V. Heine, M. T. Dove and X. Chen, *Phys. Chem. Miner.*, 1991, **18**, 326–336.
50 M. A. Carpenter, E. K. H. Salje, A. Graeme-Barber, B. Wruck, M. T. Dove and K. S. Knight, *Am. Mineral.*, 1998, **83**, 2–22.
51 A. L. Goodwin, B. J. Kennedy and C. J. Kepert, *J. Am. Chem. Soc.*, 2009, **131**, 6334–6335.
52 Z. G. Nicolaou and A. E. Motter, *Nat. Mater.*, 2012, **11**, 608–613.
53 R. Lakes and K. W. Wojciechowski, *Phys. Status Solidi B*, 2008, **245**, 545–551.
54 D. A. Woodcock, P. Lightfoot, P. A. Wright, L. A. Villaescusa, M.-J. Dìaz-Cabañas and M. A. Camblor, *J. Mater. Chem.*, 1999, **9**, 349–351.
55 K. W. Chapman, P. J. Chupas and C. J. Kepert, *J. Am. Chem. Soc.*, 2005, **127**, 15630–15636.
56 Y. Wu, A. Kobayashi, G. J. Halder, V. K. Peterson, K. W. Chapman, N. Lock, P. D. Southon and C. J. Kepert, *Angew. Chem.*, 2008, **120**, 9061–9064.
57 W. Zhou, H. Wu, T. Yildirim, J. R. Simpson and A. R. Hight Walker, *Phys. Rev. B*, 2008, **78**, 054114.
58 Y.-S. Wei, K.-J. Chen, P.-Q. Liao, B.-Y. Zhu, R.-B. Lin, H.-L. Zhou, B.-Y. Wang, W. Xue, J.-P. Zhang and X.-M. Chen, *Chem. Sci.*, 2013, **4**, 1539–1546.
59 R. Shang, G.-C. Xu, Z.-M. Wang and S. Gao, *Chem.–Eur. J.*, 2014, **20**, 1146–1158.
60 Z. Wang, B. Zhang, K. Inoue, H. Fujiwara, T. Otsuka, H. Kobayashi and M. Kurmoo, *Inorg. Chem.*, 2007, **46**, 437–445.
61 C. Mellot-Draznieks, C. Serre, S. Surblé, N. Audebrand and G. Férey, *J. Am. Chem. Soc.*, 2005, **127**, 16273–16278.
62 S. Surblé, C. Serre, C. Mellot-Draznieks, F. Millange and G. Férey, *Chem. Commun.*, 2006, 284–286.
63 L. Carlucci, G. Ciani, D. M. Proserpio and A. Sironi, *J. Chem. Soc., Chem. Commun.*, 1994, 2755–2756.
64 L. R. MacGillivray, S. Subramanian and M. J. Zaworotko, *J. Chem. Soc., Chem. Commun.*, 1994, 1325–1326.
65 J. Zhang, S. Chen and X. Bu, *Angew. Chem., Int. Ed.*, 2008, **47**, 5434–5437.
66 T. Otieno, S. J. Rettig, R. C. Thompson and J. Trotter, *Inorg. Chem.*, 1993, **32**, 1607–1611.
67 L. Ma, Y.-C. Qiu, G. Peng, J.-B. Cai and H. Deng, *Eur. J. Inorg. Chem.*, 2011, **2011**, 3446–3453.
68 N. Masciocchi, S. Galli, A. Sironi, E. Cariati, M. A. Galindo, E. Barea, M. A. Romero, J. M. Salas, J. A. R. Navarro and F. Santoyo-González, *Inorg. Chem.*, 2006, **45**, 7612–7620.
69 J. Zhang, T. Wu, C. Zhou, S. Chen, P. Feng and X. Bu, *Angew. Chem., Int. Ed.*, 2009, **48**, 2542–2545.

